

Geochemistry, Geophysics, Geosystems

RESEARCH ARTICLE

10.1029/2019GC008667

Special Section:
Polar region geosystems

Key Points:

- This study reports the first apatite (U-Th-Sm)/He data from western Marie Byrd Land
- Thermal history modeling indicates diachronous Late Cretaceous-Paleogene cooling in response to different tectonic processes
- Erosion surfaces in West Antarctica formed diachronously from west to east after 70 Ma

Supporting Information:
• Supporting Information S1

Correspondence to:
M. Zundel,
zundel@uni-bremen.de

Citation:
Zundel, M., Spiegel, C., Lisker, F., & Monien, P. (2019). Post mid-Cretaceous tectonic and topographic evolution of western Marie Byrd Land, West Antarctica: Insights from apatite fission track and (U-Th-Sm)/He data. *Geochemistry, Geophysics, Geosystems*, 20, 5831–5848. <https://doi.org/10.1029/2019GC008667>

Received 29 AUG 2019

Accepted 2 OCT 2019

Accepted article online 26 OCT 2019

Published online 6 DEC 2019

©2019. The Authors.

This is an open access article under the terms of the Creative Commons Attribution License, which permits use, distribution and reproduction in any medium, provided the original work is properly cited.

Post Mid-Cretaceous Tectonic and Topographic Evolution of Western Marie Byrd Land, West Antarctica: Insights from Apatite Fission Track and (U-Th-Sm)/He Data

Maximilian Zundel¹ , Cornelia Spiegel¹ , Frank Lisker¹ , and Patrick Monien² 

¹Geodynamics of Polar Regions, Department of Geosciences, University of Bremen, Bremen, Germany, ²Petrology of the Ocean Crust, Department of Geosciences, University of Bremen, Bremen, Germany

Abstract New low-temperature thermochronological data from granitic basement of western Marie Byrd Land (MBL) provide insights into the still poorly constrained tectonic and topographic evolution of West Antarctica during and after continental breakup. Here, we present the first apatite (U-Th-Sm)/He data from the Devonian Ford Granodiorite and the mid-Cretaceous Byrd Coast Granite suites from the Ford Ranges and the Edward VII Peninsula. Thermal history modeling integrating apatite (U-Th-Sm)/He dates of 109–68 Ma with revised apatite fission track data in combination with geologic information indicates a thermal history with diachronous enhanced cooling at ~100–60 Ma and subsequent slow cooling until the present day. Enhanced cooling at ~100–70 Ma was related to activity of the West Antarctic rift system and to continental breakup, thereby exhuming most samples to shallow crustal levels. Localized cooling at ~75–60 Ma is interpreted as resulting from faulting in the eastern Ross Sea region. Slow cooling after ~70–60 Ma corresponds with formation of erosion surfaces in western MBL. Comparison of our results from western MBL with data from the literature indicates progressive formation of erosion surfaces from west to east along the MBL-Thurston Island crustal blocks. Late Cenozoic activity of the West Antarctic rift system and MBL dome uplift appear to have caused only minor exhumation of <1.5 km in western MBL.

1. Introduction

West Antarctica is a collage of several geologically distinctive crustal blocks, including Marie Byrd Land (MBL), Thurston Island block, Antarctic Peninsula, and Ellsworth-Whitmore Mountains block (Figure 1a; Dalziel & Elliot, 1982). Together with the crustal blocks of Zealandia, they formed a vast region along the active paleo-Pacific margin of Gondwana in Palaeozoic and Mesozoic times (Figure 1b; e.g., Mukasa & Dalziel, 2000; Pankhurst et al., 1998). Intracontinental extension of the entire region since the mid- to Late Cretaceous opened the West Antarctic rift system (WARS) and resulted in crustal thinning and the low-lying topography observed today in West Antarctica (Figure 1a; Fretwell et al., 2013; Winberry & Anandakrishnan, 2004). Major tectonic activity of the WARS occurred in the Cretaceous and since the mid-Cenozoic (Cande et al., 2000; Luyendyk et al., 2003; Siddoway, 2008). Continental breakup between the crustal blocks of West Antarctica and Zealandia initiated with seafloor spreading along the Pacific-Antarctic Ridge at ~90–83 Ma, opening the southwest Pacific Ocean (Eagles et al., 2004; Larter et al., 2002). By ~85–75 Ma, the West Antarctic erosion surface (WAES) is considered to have formed as a flat surface in coastal areas in West Antarctica (LeMasurier & Landis, 1996). The WAES is an important geomorphologic feature for understanding the post-breakup evolution, which is in turn vital to constrain early glaciation in West Antarctica. The WAES also forms a unique regional marker in West Antarctica which is used to determine regional uplift because it formed at sea level (LeMasurier, 2008). The WAES truncates >85 Ma plutonic rocks in MBL which provide a maximum age constraint for the WAES formation (LeMasurier & Landis, 1996). However, a minimum age for the formation of the WAES is only indirectly constrained from correlative outcrops in New Zealand where a similar erosion surface is overlain by ~75 Ma strata (Landis et al., 2008; LeMasurier & Landis, 1996). Direct minimum age constraints on the formation of the WAES are so far lacking which is largely because 98% of the outcrops in West Antarctica are perennially ice-covered and thus not accessible for direct geological investigations. The timing of formation and uplift of the WAES and whether it formed as a single or as multiple surfaces has major consequences for onset and development of continental glaciation and is therefore the principal objective of this study.

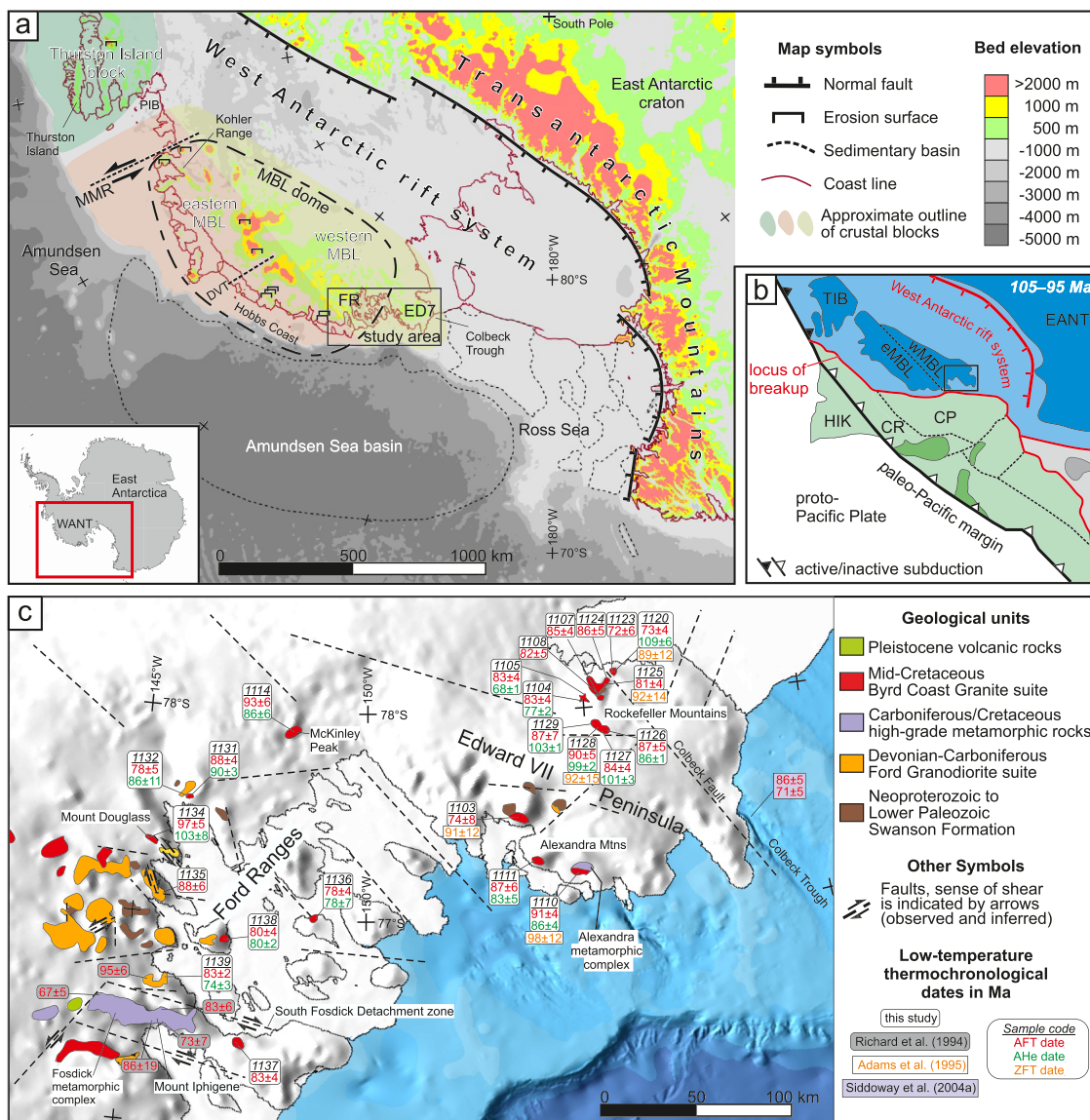


Figure 1. (a) Topographic map of the West Antarctic rift system. The location of the map on the Antarctic continent is shown in the inset. Onshore topography, the outline of the MBL-dome, contours of offshore sedimentary basins, erosion surfaces, and tectonic structures of the large map are compiled from the literature (Fretwell et al., 2013; Holschuh et al., 2014; LeMasurier, 2008; LeMasurier & Landis, 1996; LeMasurier & Rocchi, 2005; Lindeque et al., 2016; Spiegel et al., 2016; Wilson & Luyendyk, 2009). Map also shows the Thurston Island block and the crustal block of Marie Byrd Land, which can be subdivided by geochemical evidence in an eastern and a western province (Pankhurst et al., 1998). (b) Paleogeographic situation of the paleo-Pacific margin of Gondwana and tectonic plates of Antarctica (blue), Zealandia (green), and the Tasmanides (gray) at ~105–95 Ma (Gohl et al., 2013; Yakymchuk et al., 2013). Present-day continental shelves are shown in light colors; emergent land is dark colored. (c) Physiographic map of the Edward VII Peninsula and the Ford Ranges with ice- and snow-covered areas (white-gray), adjacent shelf (light blue), and deep-sea areas (deep blue) (Arndt et al., 2013). Map also shows geological units and tectonic structures (Ferraccioli et al., 2002; Lisker & Olesch, 1998; Luyendyk et al., 2001, 2003; Siddoway, 2008). Samples and results of this study are compiled with published low-temperature thermochronological data. Mean AHe dates are reported with standard deviations. CP = Campbell Plateau; CR = Chatham Rise; DVT = DeVicq trough; EANT = East Antarctica; ED7 = Edward VII Peninsula; eMBL = eastern Marie Byrd Land; FR = Ford Ranges; HIK = Hikurangi Plateau; MBL = Marie Byrd Land; MMR = Mount Murphy Rift; PIB = Pine Island Bay; TIB = Thurston Island block; WANT = West Antarctica; wMBL = western Marie Byrd Land.

A key area to pursue this objective is western MBL, which is situated within the WARS and adjacent to the former locus of breakup, while flat mountain tops may be considered as remnants of the WAES. Rifting, breakup, and erosion surface formation are usually associated with changes in exhumation and erosion, which is why the sedimentary record is commonly targeted to constrain rate and timing of associated processes. In western MBL, however, the lack of such sediments obligates to use low-temperature (LT)

thermochronological dating of *in situ* bedrock in order to monitor and constrain erosional and shallow crustal tectonic processes (e.g., Lisker et al., 2009; Summerfield & Brown, 1998). Main exposures in western MBL are located on the Edward VII Peninsula and in the Ford Ranges where they only offer a small range of relief (<1,000 m). Deciphering the geological processes active during exhumation and topographic evolution of western MBL from *in situ* and dredged bedrock samples have been the goal of several studies including zircon U-Pb geochronology, Rb-Sr geochronology, Ar-Ar high-temperature (HT) thermochronology as well as zircon and apatite LT thermochronology (e.g., Adams et al., 1995; Korhonen et al., 2010; Lisker & Olesch, 1998; McFadden et al., 2015; Richard et al., 1994; Siddoway et al., 2004a). Mid-Cretaceous to Eocene LT thermochronological dates were often interpreted to represent two discrete Late Cretaceous cooling events. However, the proposed cooling histories rely on apatite fission track (AFT) data alone, and they either do not include thermal history modeling at all or they apply outdated analytical approaches and annealing algorithms. For this study, we revise AFT data from the Edward VII Peninsula and the Ford Ranges published by Lisker and Olesch (1998) by (i) including the kinetic indicator Dpar which provides important information about the annealing behavior of apatite; (ii) using standard etching protocols and c-axis projection for length measurements (Ketcham et al., 2007a); and (iii) applying thermal history modeling with up-to-date annealing algorithms. Dpar is measured geometrically as it represents a geometrical etch figure formed by the intersection of a fission track and the c-axis parallel polished and etched apatite surface (Carlson et al., 1999; Donelick et al., 2005). Finally, we obtained the first apatite (U-Th-Sm)/He (AHe) data of western MBL and integrated them with the revised AFT data by thermal history inversions. This allows us to comprehensively reconstruct the regional cooling history since the mid-Cretaceous, to infer the upper crustal tectonic and topographic evolution, and to relate this evolution to surface and climatic processes.

2. Geological Setting

2.1. Tectonic Evolution of MBL

The crustal block of MBL belonged to a terrane-assemblage forming part of the active paleo-Pacific margin of Gondwana over large periods during the Palaeozoic and Mesozoic (Figure 1b). Neoproterozoic to Cambrian turbiditic sequences were deposited along the entire margin. These sequences were deformed and metamorphosed to low-grade conditions in the early Paleozoic and are exposed as the Swanson Formation in MBL (Figure 1c; Adams et al., 1986; Pankhurst et al., 1998). Plutonic bodies of the Ford Granodiorite suite intruded the Swanson Formation along the subduction margin in the Devonian–Carboniferous and form nowadays exposures in the Ford Ranges (Figure 1c; Siddoway & Fanning, 2009; Yakymchuk et al., 2015). Parts of both the Swanson Formation and the Ford Granodiorite suite underwent two episodes of granulite-facies metamorphism during the Devonian–Carboniferous and in the mid-Cretaceous (Korhonen et al., 2010, 2012; Siddoway & Fanning, 2009; Yakymchuk et al., 2013). The corresponding high-grade metamorphic rocks are exposed in the Ford Ranges as the Fosdick metamorphic complex and on the Edward VII Peninsula as the Alexandra metamorphic complex (Figure 1c; McFadden et al., 2010; Pankhurst et al., 1998; Smith, 1996). Voluminous batholiths of the Byrd Coast Granite suite intruded both the Swanson Formation and the Ford Granodiorite suite within two major pulses: (i) I-type subduction-related plutonism constrained to 142–110 Ma and (ii) back-arc-related alkalic intrusions, emplaced at ~115–103 Ma in the Ford Ranges (Korhonen et al., 2010; Siddoway et al., 2004a; Weaver et al., 1992, 1994) and at ~105–95 Ma on the Edward VII Peninsula (Adams et al., 1995; Siddoway, et al., 2004a).

The overall tectonic regime along the paleo-Pacific margin changed from convergence to extension sometime in the mid-Cretaceous with ENE-WSW dextral transtension in western MBL (Siddoway, 2008; Siddoway et al., 2005). The cause for this change is still under debate, while three alternative options are discussed: (i) the collision of the Hikurangi Plateau with the subduction margin at ~110–105 Ma (Figure 1b; Davy, 2014; Davy et al., 2008), (ii) the collision or interaction of a spreading ridge with the subduction margin (Lawver & Gahagan, 1994; Luyendyk, 1995; Sutherland & Hollis, 2001), and (iii) the presence of a mantle plume (Storey et al., 1999; Weaver et al., 1994). In any case, mid-Cretaceous crustal extension of the WARS was associated with granulite facies metamorphism and crustal anatexis, with compressed isotherms in western MBL (Richard et al., 1994; Yakymchuk et al., 2013). This setting triggered the intrusion of the Byrd Coast Granite suite at ~115–95 Ma (Brown et al., 2016) and the rapid exhumation of shallow to mid-crustal rocks between ~102 and 94 Ma (McFadden et al., 2015; Richard et al., 1994; Siddoway et al., 2004b). Over the same interval, metamorphic core complexes developed in Zealandia and the opening of the Tasman Sea

commenced in contiguous areas of east Gondwana. A short time later, extension between Zealandia (Campbell Plateau, Chatham Rise) and West Antarctic (e.g., MBL and Thurston Island block) occurred, leading to onset of seafloor spreading between 90 and 83 Ma (Figure 1b; Eagles et al., 2004; Larter et al., 2002). This continental breakup was accompanied by increasing erosion and deposition of large volumes of sediments in the Amundsen Sea basin that evolved between the Pacific-Antarctic Ridge and the passive margin of West Antarctica (Lindeque et al., 2016). In contrast, no Late Cretaceous–Eocene sedimentary strata crop out in onshore MBL (Pankhurst et al., 1998; Siddoway, 2008).

At ~85–75 Ma, the WAES and its equivalents started to bevel coastal batholiths in MBL and Zealandia (LeMasurier & Landis, 1996).

Renewed WARS activity since the Eocene/Oligocene was associated with exhumation of the Transantarctic Mountains forming the rift shoulder, as well as with extension and seafloor spreading in the Ross Sea sector of the rift and strike-slip movements in the Amundsen and Bellingshausen sectors of the rift (Cande et al., 2000; Müller et al., 2007; Prenzel et al., 2013, 2014; Spiegel et al., 2016). From ~30–28 Ma onward, MBL was affected by intense bimodal alkaline volcanism and uplift of the MBL dome, which has an area of 700 × 500 km and an altitude reaching 2,700 m above sea level (Figure 1c; LeMasurier, 2008). However, new thermochronological evidence from the Kohler Range and the Hobbs Coast area shows that dome uplift may have started at ~20 Ma (Spiegel et al., 2016).

2.2. Glacial History of West Antarctica

The first formation of large ice sheets in Antarctica has supposedly commenced at the Eocene-Oligocene boundary, corresponding to a global temperature decrease (Barker et al., 2007; Carter et al., 2017; Ivany et al., 2006; Zachos et al., 2001). Since the Oligocene/Miocene, continental-scale ice sheets are considered to have formed by expansion and coalescence of individual ice sheets to eventually form the West Antarctic Ice Sheet (Barker et al., 2007; Barker & Camerlenghi, 2002; Galeotti et al., 2016; Spiegel et al., 2016; Wilson et al., 2013). Today, glacial systems in eastern MBL are undergoing accelerating thinning and high mass losses, while glaciers in western MBL seem far less affected by these processes (Lindow et al., 2014; Pritchard et al., 2009; Rignot et al., 2008; Stone et al., 2003).

3. Sampling and Methods

3.1. Sampling

The 24 samples for this study were collected during the GANOVEX VII expedition of the German Federal Institute for Geosciences and Natural Resources (BGR) in 1992/1993 from nunataks of two different areas: (i) Edward VII Peninsula and (ii) Ford Ranges (Figure 1c). The samples of the Edward VII Peninsula were taken from the mountain ranges of the Alexandra and Rockefeller Mountains. Owing to outcrop conditions, samples were mostly collected from isolated nunataks. They cover an elevation range from 210 to 870 m on the Edward VII Peninsula and from 230 to 950 m in the Ford Ranges (Table S1). All samples are granites from the mid-Cretaceous Byrd Coast Granite suite, with the exception of one granodiorite sample (1139) from the Devonian Ford Granodiorite suite.

3.2. AFT Thermochronology

AFT thermochronology is a temperature-sensitive radiogenic dating method based on the spontaneous decay of ^{238}U causing lattice defects (fission tracks) within apatite crystals. Annealing of fission tracks occurs normally in the temperature interval of ~120–60 °C, which is why AFT thermochronology records geodynamic processes of the upper ~5–2 km of the continental crust. Fission tracks constantly accumulate over time, allowing to estimate time, amount, and rate of rock cooling with respect to specific temperatures in the upper crust. Based on diffusion, fission tracks anneal at ~120 °C. In the temperature range of ~120–60 °C, however, fission tracks are partially preserved (referring to the partial annealing zone; Wagner et al., 1989). Fission track shortening within the partial annealing zone provides information on the style and rate of cooling. Specific annealing temperatures depend on the chemical composition of apatite, which in turn is reflected by the etching velocity. Thus, the mean diameter of fission track etch pits parallel to the crystallographic c-axis (Dpar) is used as kinetic indicator for track annealing (Donelick et al., 2005).

Apatites of samples with published FT dates (Lisker & Olesch, 1998) were mounted and etched under current standard laboratory procedures, that is, for 20 s with 5 M HNO₃ (Ketcham et al., 2007a). Mounts were then analyzed to obtain track length data and corresponding angles to the crystallographic c-axis as well as Dpar values. Details on the laboratory procedures for AFT thermochronology are given in the supporting information.

3.3. Apatite (U-Th-Sm)/He Thermochronology

AHe thermochronology is based on the production of radiogenic ⁴He as a daughter isotope of ²³⁸U, ²³⁵U, ²³²Th, and ¹⁴⁷Sm. Diffusion in apatite at temperatures >85 °C leads to ⁴He loss. ⁴He is partially retained at temperatures between ~85 and 40 °C (referring to the He partial retention zone) and mostly accumulates at temperatures <40 °C (Wolf et al., 1998). Hence, AHe thermochronology records upper crustal dynamics at ~3–1 km crustal depths. In addition to temperature-dependent diffusional loss, ⁴He is lost from the grain by alpha-ejection along the outer ~20 µm rim of the apatite grain, independent from temperature (Farley et al., 1996). To adjust for this effect, AHe raw dates in this study were corrected according to size and morphology of the analyzed grain, using the stopping distances of Ketcham et al. (2011). Apatites for AHe thermochronology were selected from samples of the study of Lisker and Olesch (1998). Details on the laboratory procedures for AHe thermochronology are given in the supporting information.

3.4. Thermal History Modeling

For thermal history modeling, we used the annealing algorithm of Ketcham et al. (2007b) for AFT data. For AHe data, we used the He diffusion algorithm for Durango apatite of Farley (2000) and the algorithm RDAAM of Flowers et al. (2009). These algorithms are based on the experimentally determined fission track annealing and helium-diffusion behavior in apatite. The computer program HeFTy uses these equations to extrapolate the annealing and diffusion over geologic time scales (Ketcham, 2005). For this study, we used HeFTy (version 1.8.3) to inversely produce continuous time-temperature paths (t-T paths), which were based on coupled AFT and AHe dates in combination with data of track length distribution and Dpar. For modeling, track lengths were projected to the c-axis of corresponding apatite crystals (Ketcham et al., 2007a). Because Dpar values are very homogeneous, AFT dates of Lisker and Olesch (1998) were modeled with mean Dpar values obtained from track length measurements. Nineteen samples selected for modeling comprise more than 70 length measurements of horizontal confined tracks. Fifteen models were supplemented by AHe data. For each sample, 100,000 paths were generated and tested. HeFTy compares modeled and observed thermochronological data and characterizes their match by a “goodness-of-fit” parameter (GOF). Resulting “acceptable” paths have a GOF >0.05, and “good” paths have GOF >0.5. Good paths are in agreement with the sample data, while acceptable paths are not ruled out by the sample data. A comparison of measured and modeled data is shown in Table S5.

4. Thermochronology

4.1. Published Thermochronological Data of Western MBL

HT thermochronological dating (e.g., K-Ar and Ar-Ar) of rocks of the Ford Ranges and Edward VII Peninsula predominantly yielded mid-Cretaceous ages (Adams et al., 1995; McFadden et al., 2015; Richard et al., 1994; Siddoway, et al., 2004a). These ages closely correspond with published LT thermochronology dates. Lisker and Olesch (1998) obtained AFT dates of 97–72 Ma from the Edward VII Peninsula and the Ford Ranges (see section 4.2). These AFT dates and the corresponding samples were used for thermal modeling and for AHe analysis in the present study. Other AFT dates from locations in the Ford Ranges vary between 95 and 67 Ma (Richard et al., 1994) and between 77 and 56 Ma on the Edward VII Peninsula (Adams et al., 1995). Two AFT dates of 86 and 71 Ma were obtained from dredged samples in the Colbeck Trough offshore Edward VII Peninsula (Siddoway, et al., 2004a). Published MTL data mostly vary between 13 and 14 µm with standard deviations of 1.0 to 2.0 µm (Adams et al., 1995; Richard et al., 1994; Siddoway, et al., 2004a). Adams et al. (1995) published zircon fission track dates of 98–83 Ma from locations in the Edward VII Peninsula. Single grain zircon (U-Th)/He dates of 88–73 and 98–67 Ma and single grain apatite (U-Th)/He dates of 87 and 78 Ma, respectively, are reported for the Edward VII Peninsula and the Ford Ranges, respectively (Contreras et al., 2011). The bulk zircon fission track, AFT, and AHe dates of western MBL outline a date-elevation pattern which is characterized by a broad spectrums of dates for elevations ~200–600 m and thus no clear relationships (Figure S4).

4.2. AFT Data: Previous and Revised

Twenty-four AFT dates from the Edward VII Peninsula and the Ford Ranges range from 97 ± 5 to 72 ± 6 Ma (Table 1; Figure 2). At a similar relief difference of ~ 700 m, with most samples originating from 400–700 m elevations, the spread in AFT dates within the two sampling areas is comparable: samples of the Edward VII Peninsula range over 91–72 Ma and in the Ford Ranges over 97–78 Ma. All AFT dates are concordant with or slightly younger than the ~ 115 –95 Ma intrusion ages of the Byrd Coast Granite suite (Adams et al., 1995; Korhonen et al., 2010; Siddoway, et al., 2004a; Siddoway & Fanning, 2009; Yakymchuk et al., 2013). AFT dates show no clear spatial distribution (Figure 1c). However, a tentative exception are two out of three samples (1120 and 1123) with the youngest AFT dates (< 75 Ma) which originate from the southernmost outcrops on the Edward VII Peninsula (Figure 1c). Nineteen samples pass the χ^2 -test, indicating that grains represent a single age population. Four samples (1111, 1123, 1127, and 1137) fail the χ^2 -test at the 5% level which indicates that these samples refer to a mixed age population. Revised MTL values of samples range from 13.1 ± 0.2 to 14.2 ± 0.1 μm with standard deviations of 1.0 to 1.8 μm (Table 1). MTL differ from the previous measurements of Lisker and Olesch (1998) by ± 0.8 μm . Track length distributions of all samples are unimodal to slightly negatively skewed (Figure S1). Relatively small Dpar values of 1.4–1.8 μm with only little variations indicate relatively similar fast-annealing apatite for all samples (Carlson et al., 1999). Edward VII Peninsula samples from elevations > 400 m show AFT dates of 91–80 Ma, which show a weak positive trend with sample elevation, except for 1110 which is slightly offset from this trend (Figure 2a). In contrast, three samples (1103, 1120, and 1123) from elevations < 400 m show younger AFT dates of 74–72 Ma (Figure 2a). A tentative positive correlation of MTL values with sample elevation is observed for most Edward VII Peninsula samples (Figure 2b). Three samples (1104, 1111, and 1128), however, deviate from this correlation (Figure 2b). Samples from the Ford Ranges show a weak AFT date-elevation correlation, from which 1114 and 1134 are offset toward older dates (Figure 2c). MTL values from Ford Ranges samples show no clear trend with sample elevation (Figure 2d).

4.3. Apatite (U-Th-Sm)/He Data

AHe data comprise nine samples from the Edward VII Peninsula and seven from the Ford Ranges (Table 2; Figures 2a and 2c). Single grain AHe dates of all samples range from 114 ± 6 to 67 ± 3 Ma with variable intra-sample date dispersions of up to 24 Myr. Mean AHe dates were calculated from two to five single grain dates per sample and were reported with standard deviations (Table 2). Mean AHe dates of all samples range from 109 ± 8 to 68 ± 1 Ma. Most samples of the Edward VII Peninsula and all samples from the Ford Ranges show overlapping mean AHe and AFT dates, considering 1σ error. Only sample 1105 shows a mean AHe date which is distinctly younger than the corresponding AFT date (Figure 2a). Four samples (1120, 1127, 1128, and 1129) of the Edward VII Peninsula yield a crossover relationship, which means that mean AHe dates are older than the corresponding AFT dates within error limits (e.g., Spiegel et al., 2009). Crossover AHe dates preclude a straightforward interpretation. Since these crossover dates, however, are well replicating, fairly overlapping with K-Ar ages from the same locations (Adams et al., 1995), and their U-Th-Sm chemistry is not distinct from most other samples, we do not completely exclude that they may be geologically meaningful, but we did not use them as basis for thermal history inversions. The effective U concentration (eU) of analysed apatite grains in general varies between 9 and 77 ppm (Table 2). Intrasample eU dispersion is relatively small which is why the effect of eU zonation on the AHe date calculation is probably minor. Samples with crossover dates show no obvious correlations of date and eU or date and grain radius, respectively (Figures S2a and S2b). Samples 1111 and 1114 reveal positive date-eU correlations (Figure S2). This correlation may indicate a potential influence of radiation damage on He retentivity of apatite (Flowers et al., 2007). Despite this potential influence, these samples show relatively small date dispersions, which suggests rather rapid cooling (Flowers & Kelley, 2011). A weak inverse correlation of AHe date and grain radius is observed for samples 1110 and 1132 (Figures S2c and S2d). This correlation may be explained by ${}^4\text{He}$ implantation from adjoining minerals rich in U-Th-Sm (Spiegel et al., 2009). Microscopical analysis in these samples revealed indeed biotite and epidote in association with apatite.

4.4. Thermal History Models

Inverse thermal history modeling relies on both AFT and AHe data and external t-T constraints. In general, the starting t-T constraint of the samples is provided by geochronological and thermochronological dates and their corresponding closure temperatures > 200 °C (Table S4). Modeling of some samples of the Ford

Table 1

Results of apatite fission track (AFT) analyses. Central AFT dates are from Lisker and Olesch (1998), track length and Dpar measurements are results of this study

Code	Location	Elevation m	n	Nd	pd	Ns	ps	Ni	pi	P(X) ² %	Central AFT dates Ma ($\pm 1\sigma$)	U ppm	MTL $\mu\text{m} (\pm 1\sigma)$	SD μm	nMTL	Dpar $\mu\text{m} (\pm 1\sigma)$
Edward VII Peninsula																
1103	Bowmans Peak	300	20	7759	12.78	161	0.103	490	0.297	45	74 \pm 8	1	-	-	-	
1104	Mount Paterson	540	32	7759	12.78	915	0.621	2442	1.63	83	83 \pm 4	5	13.1 \pm 0.17	1.64	99	1.47 \pm 0.14
1105	Mount Paterson	450	34	7759	12.78	1125	0.931	3012	2.45	27	83 \pm 4	7	13.3 \pm 0.15	1.47	97	1.50 \pm 0.12
1107	Mount Nilson	700	24	7759	12.78	2076	1.16	5418	3.06	9	85 \pm 4	8	13.4 \pm 0.12	1.22	101	1.75 \pm 0.14
1108	Strider Rock	620	28	7759	12.78	1001	0.622	2740	1.67	9	82 \pm 5	5	13.4 \pm 0.34	1.71	25	1.44 \pm 0.13
1110	Prestrup Rock	620	20	7759	12.78	3222	2.66	7884	6.54	17	91 \pm 4	18	13.5 \pm 0.14	1.45	105	1.69 \pm 0.14
1111	Mount Swadener	420	8	7759	12.78	2172	3.57	5522	9.28	0	87 \pm 6	26	14.0 \pm 0.14	1.36	100	1.77 \pm 0.22
1120	Tennant Peak	285	32	7759	12.78	817	0.499	2499	1.53	82	73 \pm 4	4	13.5 \pm 0.17	1.46	71	1.47 \pm 0.11
1123	Mount Butler	210	20	7759	12.78	458	0.451	1481	1.40	0	72 \pm 6	4	13.4 \pm 0.18	1.78	99	1.42 \pm 0.16
1124	Gould Peak	450	12	7759	12.78	660	0.699	1714	1.83	86	86 \pm 5	5	-	-	-	-
1125	Breckinridge Peak	555	53	7730	12.72	1840	0.801	5080	2.20	22	81 \pm 4	6	-	-	-	-
1126	Mount Frazier	870	20	7759	12.78	567	0.434	1456	1.11	80	87 \pm 5	3	13.5 \pm 0.17	1.64	90	1.56 \pm 0.18
1127	Mount Jackling	840	48	7730	12.72	2334	0.773	6371	2.09	3	84 \pm 4	6	13.6 \pm 0.11	1.07	100	1.68 \pm 0.14
1128	Mount Fitzsimmons	850	24	7730	12.72	1345	0.812	3224	1.96	12	90 \pm 5	5	13.8 \pm 0.12	1.31	110	1.62 \pm 0.12
1129	Mount Shideler	810	16	7759	12.78	483	0.37	1220	0.968	11	89 \pm 7	3	13.4 \pm 0.16	1.39	80	1.50 \pm 0.13
Ford Ranges																
1114	McKinley Peak	620	25	7759	12.78	574	0.633	1365	1.45	22	93 \pm 6	4	13.5 \pm 0.15	1.47	97	1.44 \pm 0.17
1131	Mount Ronne	575	50	7730	12.72	2173	0.725	5547	1.81	84	88 \pm 4	5	14.2 \pm 0.11	1.05	91	1.41 \pm 0.12
1132	Mount Ronne	480	24	7730	12.72	734	1.59	2133	4.63	5	78 \pm 5	13	14.0 \pm 0.13	1.22	90	1.42 \pm 0.11
1134	Mount Douglas	600	21	7730	12.72	828	0.846	1892	2.00	91	97 \pm 5	6	13.7 \pm 0.16	1.59	100	1.54 \pm 0.22
1135	Bilboard	950	20	7730	12.72	451	0.718	1108	1.69	69	88 \pm 6	5	-	-	-	-
1136	Barela Rock	250	32	7730	12.72	904	0.437	2585	1.20	86	78 \pm 4	3	13.8 \pm 0.13	1.33	98	1.69 \pm 0.15
1137	Mitchell Peak	610	23	7730	12.72	2314	2.49	6274	6.63	1	83 \pm 4	18	13.7 \pm 0.13	1.00	53	1.44 \pm 0.15
1138	Clark Knoll	400	26	7730	12.72	1041	0.549	2884	1.51	97	80 \pm 4	4	13.8 \pm 0.17	1.66	100	1.44 \pm 0.14
1139	Chester Mountains	230	20	7730	12.72	678	0.637	1936	1.79	48	78 \pm 5	5	13.6 \pm 0.18	1.81	97	1.46 \pm 0.11

Zeta=350.5 \pm 12.3 (F.Lisker), calculated for dosimeter glass SRM612 (37.38 ppm uranium); n=number of counted grains; Nd/Ns/Ni=number of tracks on dosimeter glass/on apatite/on mica; pd/ps/pi=density of tracks (10^5 tracks/ cm^2) on dosimeter glass/on apatite/on mica; P(X)²=probability, where P(X)²>5% indicates a single-age population (Galbraith, 1981); central AFT dates were calculated using software TRACKKEY (Dunkl, 2002); 1 σ errors=conventional method (Green, 1981); U=uranium content; MTL=mean track length (non-c-axis corrected values); SD=standard deviation; nMTL=number of measured track lengths; Dpar=kinetic parameter.

Ranges without such age data start with a generous initial constraint at \sim 300 °C and 115–95 Ma. Finally, we let the samples cool to temperatures of 0 °C. All t-T constraints were integrated in 19 inverse HeFTy models to identify timing of cooling periods. All models show a relatively similar two-stage cooling pattern with enhanced cooling in the mid- to Late Cretaceous and slow cooling thereafter (Figures 3 and S3). The timing of enhanced cooling is, however, diachronous and occurred during two, partially overlapping periods for each of the Edward VII Peninsula and the Ford Ranges (Figure 3).

4.4.1. Edward VII Peninsula

Cooling stage 1:

- a Enhanced cooling occurred within the period ~102–80 Ma at rates of 6–23 °C/Myr through the temperature window of ~120 °C to 30–65 °C (end of enhanced cooling of individual samples) (Figure 3a). This cooling period is recorded by most samples from the Edward VII Peninsula. Higher, more variable cooling rates of this cooling period of 9–180 °C/Myr are derived by integrating from temperatures of \sim 300 °C to 30–65 °C between ~103 and 80 Ma based on K-Ar biotite data (Adams et al., 1995) and our thermal

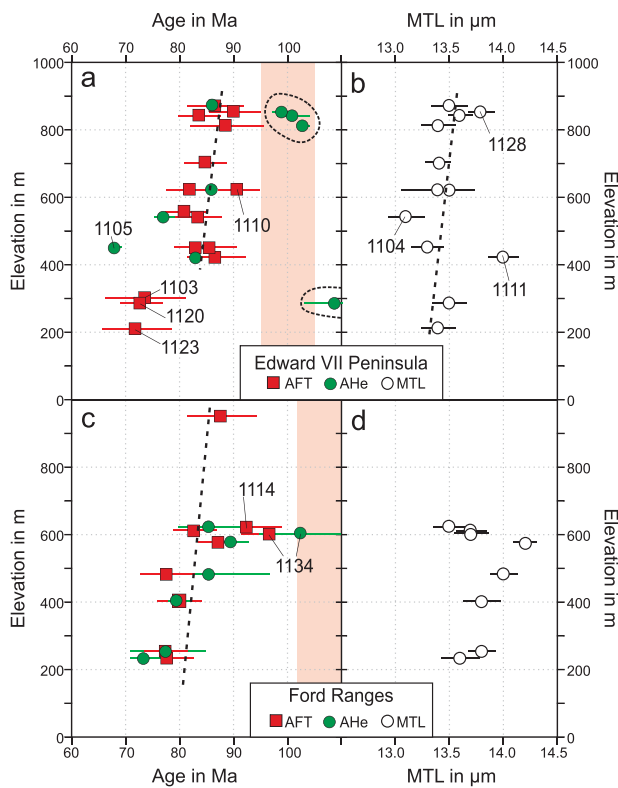


Figure 2. Relationship between apatite fission track (AFT) dates, mean (U-Th-Sm)/He (AHe) dates, mean track length (MTL) values, and sample elevations from Edward VII Peninsula (a, b) and Ford Ranges (c-d). Horizontal lines refer to 1σ errors (red and black) and standard deviations (green). The red shadow corresponds with the intrusion ages of the Byrd Coast Granite suite (Adams et al., 1995; Richard et al., 1994; Siddoway et al., 2004a). Dashed line outlines date-elevation or MTL-elevation trends, respectively. Crossover AHe dates overlapping with intrusion ages are encircled by dotted line. The labelled data points refer to descriptions in the text.

5. Discussion

5.1. Late Cretaceous Granite Intrusion and Exhumation

Thermal history modeling of all samples in this study suggest that the currently exposed rocks of western MBL cooled from temperatures >120 °C to near-surface temperatures during mid- to Late Cretaceous and Paleocene times (Figure 4). Mostly overlapping AFT and AHe dates of this study and the close correspondence of LT and HT thermochronological data as well as the overlap of cooling ages with U-Pb zircon crystallization ages of the Byrd Coast Granite suite (e.g., Korhonen et al., 2010; McFadden et al., 2015; Siddoway et al., 2004a) point to continuous rapid cooling of western MBL from temperatures >800 °C to <100 °C for the time interval ~ 105 – 90 Ma (Figure 4a). Thus, onset of cooling of the sample's host rocks is inferred directly after granite emplacement, which relates HT cooling predominantly to thermal relaxation associated with magmatic cooling. However, LT cooling, that is, cooling to temperatures <120 °C, of plutonic rocks requires exhumation to shallow crustal levels. We therefore attribute LT cooling predominantly to exhumation. To transfer cooling during ~ 100 – 70 Ma at temperatures <120 °C into exhumation rates, we assumed geothermal gradients of 30–70 °C/km and ~ 15 °C surface temperatures for the Cretaceous (Poole et al., 2005). The chosen range of geothermal gradients allow for substantial heat-flow variations in a rifting-controlled setting and these gradients are similar to values used in adjacent regions (Lindow et al., 2016; Spiegel et al., 2016; Zundel et al., 2019). Exact intrusion depths of the Byrd Coast Granite suite are unknown but they can be estimated by petrographic observation. Miarolitic granitic varieties, smoky quartz, and subvolcanic textures of the granite samples indicate rather shallow intrusion levels of ≤ 2 kbar (e.g.,

models. The end of enhanced cooling during the 102–80 Ma cooling period is diachronous for the individual samples. Notably, samples 1128 and 1129 from the northern Rockefeller Mountains cooled to temperatures <50 °C by ~ 95 Ma, ca. 5–15 Myr earlier than the other samples (Figure 3a).

b Between ~ 75 and 60 Ma, enhanced cooling to temperatures of ~ 45 – 60 °C with rates of 6–8 °C/Myr is recorded by samples 1120 and 1123 (Tennant Peak and Mount Butler), located in the southern Rockefeller Mountains close to the Ross Sea Embayment (Figure 1c). This cooling period coincides with renewed enhanced cooling from 70 °C to 30 °C at a rate of ~ 2 °C/Myr recorded by sample 1111 (Alexandra Mountains).

Cooling stage 2:

After 60 Ma, all models favor slow cooling with similar rates (<1 °C/Myr) through to the Miocene. Slightly increased cooling may have occurred between ~ 15 Ma and the present day.

4.4.2. Ford Ranges

Cooling stage 1:

a From 100 to 88 Ma, enhanced cooling through the temperature window of ~ 120 °C to 30–45 °C at rates of ~ 11 °C/Myr is recorded by samples 1114 and 1134 (Figure 3b). These two samples originate from two isolated nunataks (Mount Douglass and McKinley Peak) in the southern Ford Ranges (Figure 1c).

b Between 87 and 70 Ma, enhanced cooling at rates of 9–14 °C/Myr to temperatures of 20–50 °C is indicated by thermal models of most samples from the broader Ford Ranges (Figure 3b).

Cooling stage 2:

After ~ 70 Ma, all samples from the Ford Ranges cooled slowly (<1 °C/Myr) until present.

In a summary, enhanced cooling is recorded by our samples over the intervals ~ 100 – 60 Ma (Edward VII Peninsula) and ~ 100 – 70 Ma (Ford Ranges).

Table 2

Results of apatite (U - Th - Sm)/He thermochronological analyses. for details about error calculation, see text S2

Sample code	Raw date	Error	Ft	^{40}He	Mass	Sm	Th	U	eU	r_{sphere}	Corr. date	Error	Mean corr. date \pm SD
Aliquot	Ma	Ma		ncc	μg	ppm	ppm	ppm	ppm	μm	Ma	Ma	Ma
Edward VII Peninsula													
Mount Paterson (540 m)													
1104													
1	59.7	0.5	0.76	0.36	4.5	114	10.8	7.57	10.7	61	79	4	77±2
3	47.6	0.5	0.63	1.86	3.5	227	69.5	26.8	44.3	41	75	4	
Mount Paterson (450 m)													
1105													
2	46.3	0.5	0.67	0.27	2.0	87.5	15.4	20.1	24.2	48	69	4	
3	44.8	0.5	0.66	1.23	1.5	83.3	21.5	26.1	31.6	45	67	3	68±1
4	41.5	0.4	0.61	0.27	1.3	107	27.5	33.4	40.4	41	68	3	
Prestrup Rock (620 m)													
1110													
1	62.1	0.4	0.72	1.27	2	87.6	6.51	71.8	73.8	52	86	4	
2	63.4	0.4	0.69	0.99	1.9	56.8	4.54	64.9	66.2	45	91	5	86±4
3	59.4	0.5	0.72	1.20	2.5	88.9	4.85	63.7	65.3	54	82	4	
Mount Swadener (420 m)													
1111													
1	67.4	0.3	0.84	6.18	12.7	88.1	4.60	57.8	59.4	93	80	4	
2	55.9	0.8	0.63	0.86	1.7	38.0	7.63	75.4	77.4	74	89	5	
3	65.8	0.4	0.78	2.73	5.6	75.0	2.98	60.1	61.2	69	84	4	83±5
4	57.1	0.7	0.76	2.24	6.3	61.2	0.649	50.8	51.3	67	75	4	
5	70.5	0.6	0.81	4.80	8.6	54.6	4.65	63.2	64.6	73	87	4	
Tenant Peak (285 m)													
1120													
1	72.0	0.7	0.70	0.56	1.9	214	35.1	23.3	32.7	50	103	5	
5	72.7	1.2	0.68	0.65	2.6	153	31.8	19.9	28.2	51	106	6	109±6
6	80.6	0.5	0.69	0.78	2.1	218	47.1	25.9	38.1	49	117	6	
Mount Frazier (870 m)													
1126													
1	61.4	0.4	0.70	0.52	2.7	159	39.1	14.9	25.0	52	88	4	
3	61.5	0.4	0.72	0.76	2.3	162	37.7	19.5	29.2	54	85	4	86±1
6	58.6	0.5	0.68	0.48	1.6	179	56.2	30.1	44.3	47	86	4	
Mount Jackling (840 m)													
1127													
3	64.3	0.4	0.65	0.68	1.5	222	61.4	42.8	58.4	44	99	5	
4	62.0	0.5	0.63	0.46	1.6	167	29.6	28.8	36.7	43	99	5	101±3
5	69.4	0.4	0.66	0.53	1.4	188	42.6	32.9	43.9	44	105	5	
Mount Fitzsommers (850 m)													
1128													
2	73.6	0.4	0.77	1.95	5.1	167	43.1	31.1	42.1	66	96	5	
3	75.5	0.4	0.75	1.90	4.3	138	40.1	22.6	32.7	57	100	5	99±2
4	78.6	0.5	0.78	1.11	5.7	95.4	14.0	16.3	20.1	65	101	5	
Mount Shideler (810 m)													
1129													
2	67.3	0.7	0.66	0.29	1.5	102	33.8	14.7	23.2	42	103	5	
3	65.6	0.5	0.63	0.84	1.7	156	60.9	46.7	61.8	43	104	5	103±1
5	66.3	0.5	0.65	0.68	1.2	191	44.5	38.8	50.2	42	102	5	
Ford Ranges													
114													
McKinley Peak (620 m)													
1	69.7	0.6	0.73	0.38	3.0	67.9	16.4	10.6	14.8	50	96	5	
2	60.5	0.5	0.71	0.31	2.7	136	29.1	7.81	15.4	50	86	4	86±6
3	52.9	0.6	0.67	0.14	2.0	108	20.2	5.17	10.5	44	79	4	
4	66.1	0.4	0.79	0.58	7.6	76.0	17.2	4.71	9.17	72	83	4	
Mount Ronne (575 m)													
1131													
1	56.5	0.4	0.66	0.17	1.2	87.9	11.7	12.8	16.1	43	86	4	
2	64.3	1.0	0.69	0.38	2.7	97.1	18.2	13.2	18.0	51	94	5	90±3
3	67.5	0.7	0.76	0.46	4.6	54.9	13.3	8.54	11.9	65	89	5	
Mount Ronne (480 m)													
1132													
1	68.7	0.7	0.68	0.32	1.6	117	23.9	18.4	24.7	51	101	5	
3	58.5	0.3	0.73	0.84	2.5	157	60.4	32.2	47.3	60	80	4	86±11
4	59.8	0.3	0.77	1.16	6.6	76.8	17.1	12.4	16.8	64	77	4	
Mt Douglas (600 m)													
1134													
2	60.0	0.6	0.59	0.22	1.0	70.2	13.8	25.7	29.3	42	95	5	
4	78.1	0.7	0.64	0.57	1.1	111	27.5	42.4	49.4	45	114	6	103±8
5	70.6	0.8	0.68	0.30	1.6	71.5	7.74	16.9	19.1	54	99	5	

Table 2
(continued)

Sample code	Raw date	Error	Ft	${}^4\text{He}$	Mass	Sm	Th	U	eU	r_{sphere}	Corr. date	Error	Mean corr. date \pm SD
Aliquot	Ma	Ma		ncc	μg	ppm	ppm	ppm	ppm	μm	Ma	Ma	Ma
1136	Barela Rock (250 m)												
1	47.1	0.5	0.69	0.16	3.1	31	22.7	3.36	8.86	54	68	3	
2	69.3	0.3	0.82	0.97	11	39	24.0	4.14	10.0	92	85	4	78\pm7
3	54.6	0.3	0.67	0.43	2.0	38	101	7.37	31.3	48	82	4	
1138	Clark Knoll (400 m)												
2	57.6	0.3	0.72	0.53	2.8	60	40.8	16.9	26.8	59	80	4	
3	59.3	0.6	0.72	0.29	3.0	34	17.1	9.45	13.7	55	82	4	80\pm2
4	52.9	0.2	0.68	0.56	2.9	59	44.6	19.3	30.1	51	78	4	
1139	Chester Mts (230 m)												
1	56.8	0.4	0.73	1.40	4.0	35	68.0	34.3	50.5	63	78	4	
2	51.8	0.6	0.69	0.23	2.0	17	15.0	7.29	10.9	52	75	4	74\pm3
4	52.4	0.4	0.75	0.41	3.8	26	26.0	10.7	16.9	62	70	4	

Ft=α-ejection correction after Farley et al. (1996); ncc=nano cubic centimeters; ppm refers to ng/mg; r_{sphere} =equivalent sphere radius of measured crystal; SD=standard deviation, all aliquots refer to single-grain measurements, eU= effective U-content ($e\text{U} = \text{U} + 0.235 \times \text{Th} + 0.0053 \times \text{Sm}$; Spiegel et al. (2016)); Figures in italics were not considered for thermal history modeling.

Candela, 1997). Because not all samples showed these features, a range of intrusion depths of 3–7 km were used for net exhumation estimations throughout this study.

5.2. Tectonic Context for Late Cretaceous Exhumation

5.2.1. West Antarctic Rift System

Samples from the Edward VII Peninsula and the Ford Ranges show LT cooling to temperatures <80 °C between ~100 and 88–80 Ma at comparable rates. This timing of LT cooling overlaps with the activity of the WARS as constrained by HT cooling and exhumation of extensional structures in western MBL between 102 and 94 Ma (Figure 4a; McFadden et al., 2015; Richard et al., 1994; Siddoway et al., 2004a). LT cooling may therefore represent a continuation of the HT cooling history (Figure 4a). LT cooling at ~100–88 Ma in the Ford Ranges is recorded by samples 1114 and 1134 which document exhumation to shallow crustal depths of 0.4–0.8 km. Sample 1134 originates from Mount Douglass that immediately borders a sinistral NW-SE-striking strike-slip shear zone (Siddoway, 2008). An inferred fault of similar orientation but of unknown kinematics is close to sample 1114 (Figure 1c). Thus, exhumation in the Ford Ranges during the interval ~100–88 Ma was likely controlled by a set of conjugate strike-slip and subordinate normal faults, which accommodated ENE-WNW-directed transtension along the extending paleo-Pacific margin (Figure 5a; Luyendyk et al., 2003; McFadden et al., 2010; Siddoway, 2008). This tectonic setting is also assumed for exhumation at 102–80 Ma for samples from the Edward VII Peninsula because of similar timing, rate, and style of cooling. Diachronous exhumation of the Edward VII Peninsula samples to shallow crustal levels is interpreted as a result of exposed different crustal levels which were laterally and vertically displaced against each other during and after exhumation. However, relatively contemporaneous exhumation to variable shallow crustal levels as shown by Edward VII Peninsula samples suggests heat-flow variations during exhumation. That local heat-flow variation had indeed an effect during exhumation is also suggested by an absolute temperature difference of ~25 °C at 80 Ma between the t-T paths of adjacent samples 1104 and 1105 (Figure 3a).

The strike-slip-dominated setting with mainly subvertical fault geometries suggests a combination of erosional and tectonic exhumation. Erosional exhumation mainly resulted from erosion of preexisting relief and relief generated along strike-slip structures while the corresponding erosional detritus was presumably deposited in syn-tectonic rift basins (Figure 5a). Tectonic exhumation was probably restricted to footwall blocks of low-angle detachment faults, for example, South Fosdick Detachment zone (Figure 1c, McFadden et al., 2010, McFadden et al., 2015). Because samples of this study originate from the hanging wall blocks, net exhumation derived from thermal histories may therefore largely result from erosion. Net exhumation during the periods ~102–80 and ~100–88 Ma totals to 1.3–6.8 and 2.2–6.6 km at rates 0.07–0.75 and 0.16–0.38 km/Myr for the samples from the Edward VII Peninsula and the Ford Ranges, respectively.

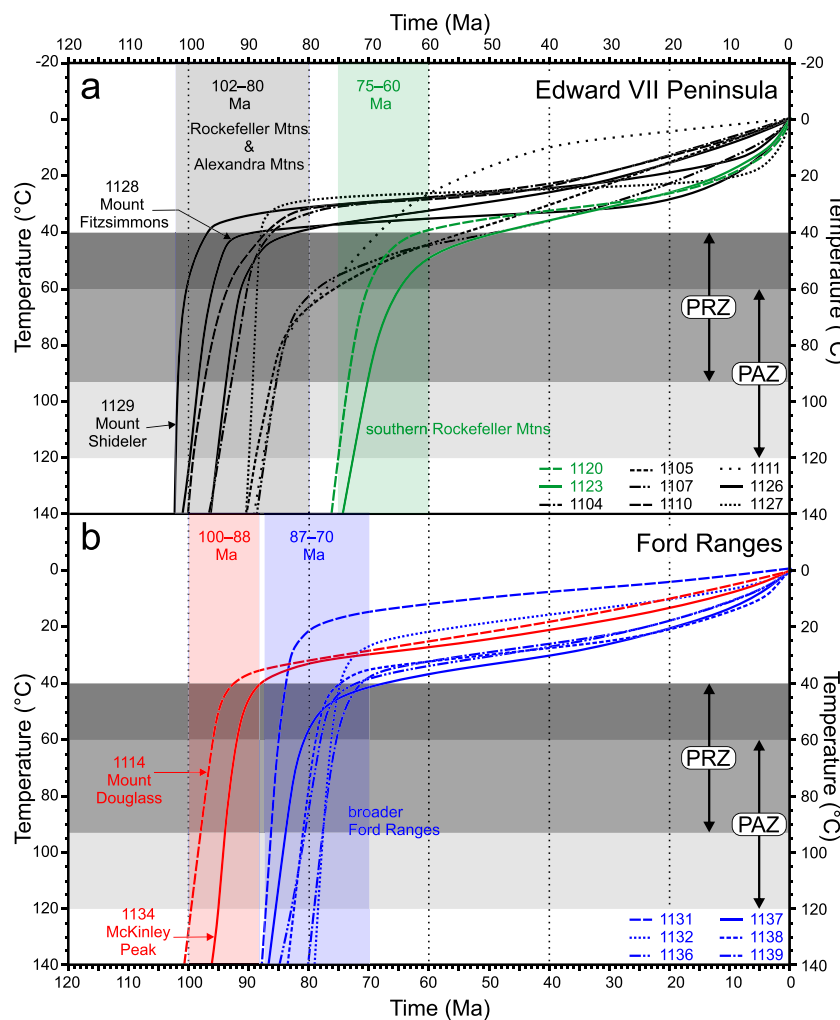


Figure 3. Thermal history inversion based on HeFTy (Ketcham, 2005) for samples of (a) Edward VII Peninsula and (b) Ford Ranges. Curves represent weighted mean cooling paths of the individual samples (see Figure S3). The cooling paths are grouped and color-coded based on their timing of enhanced cooling. Gray areas delineate the apatite partial annealing zone (PAZ) and partial retention zone (PRZ). In the PAZ and PRZ temperature ranges, the modeled results are most reliable for the applied thermochronometers. Details of the thermal history inversion are provided in the supporting information.

5.2.2. Continental Separation

Relatively rapid exhumation under relatively constant rates of 0.13–0.48 km/Myr occurred during the period 87–70 Ma in the Ford Ranges (Figure 3b). This period coincided with tectonic denudation along extensional shear zones in Zealandia at ~89–82 Ma and with onset of seafloor spreading at ~83–79 Ma between MBL and the Campbell Plateau (Kula et al., 2007; Larter et al., 2002). The locus of seafloor spreading along the Pacific–Antarctic Ridge was very close (<250 km) to the Ford Ranges (Figure 5b). This proximity and the temporal coincidence strongly indicate that exhumation in the Ford Ranges at ~87–70 Ma was predominantly driven by processes active during continental breakup. Because breakup cut across rift structures of the WARS at a high angle and only little deformation has occurred in the eastern Ross Sea during breakup (Luyendyk et al., 2001; Siddoway, 2008), we explain variable net exhumation values of ~1.8–6.9 km as resulting from mainly erosional exhumation.

5.2.3. Ross Sea Rifting

Enhanced cooling during the interval ~75–60 Ma is recorded by samples from Tennant Peak and Mount Butler which lie near cataclasite fault zones at the southeasterly extension of the Colbeck Trough (Figures 1c and 5b; Luyendyk et al., 2001). The Colbeck Trough is considered to be the morphologic expression of the NNW-trending Colbeck Fault, which initiated in the mid-Cretaceous and delineates a prominent

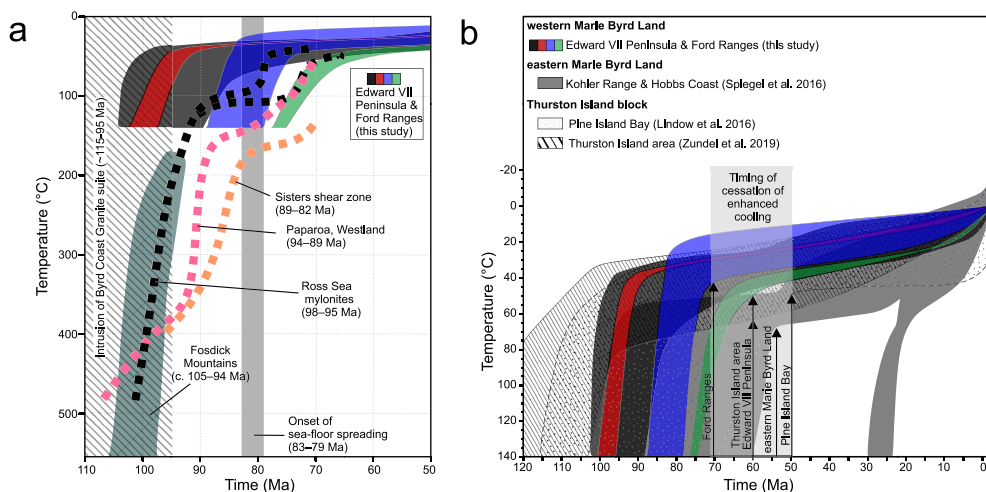


Figure 4. (a) Compilation of time-temperature paths showing low-temperature cooling of the Ford Ranges and Edward VII Peninsula (this study) together with other cooling rate and high-temperature age constraints from the literature (Adams et al., 1995; Korhonen et al., 2010; Kula et al., 2007; Larer et al., 2002; McFadden et al., 2015; Siddoway et al., 2004a; Spell et al., 2000). (b) Time-temperature plot shows cooling paths derived from the Marie Byrd Land and Thurston Island crustal blocks. The cessation of enhanced cooling is highlighted for the individual areas.

half-graben linked to the faulting in the Ross Sea sector of the WARS (Figures 1a and 1c; Ferraccioli et al., 2002; Luyendyk et al., 2001). Next to mid-Cretaceous fault activity, Luyendyk et al. (2001) indicated that later faulting occurred prior to the late Oligocene. According to thermal history modeling of this study, exhumation of ~3–1 km (for geothermal gradients of 30–60 °C/km) at ~75–60 Ma may be explained by fault activity along the Colbeck Fault (Figure 5b). The linear trend of the Colbeck Fault, however, suggests that it may be a wrench structure, in that case, exhumation is either attributed to small amounts of tectonic exhumation of the slightly dipping hanging wall or more likely to efficient erosion of the weakened fault rocks. Exhumation at ~75–60 Ma is also in agreement with an AFT date of 71 Ma and a relatively high MTL value from a dredged sample from the Colbeck Trough (Figure 1c; Siddoway et al., 2004a). The timing of exhumation coincides with extension of up to 200 km at ~68–46 Ma between East and West Antarctica and associated rifting in the Ross Sea region (Cande & Stock, 2004; Wilson & Luyendyk, 2009). Alternatively, activity of the Colbeck Fault at ~75–60 Ma as a sinistral strike-slip fault would be compatible with Campbell Plateau-MBL breakup.

5.3. Formation of Erosion Surfaces in West Antarctica

Relatively rapid exhumation in western MBL terminated at ~70 Ma in the Ford Ranges and at ~60 Ma on Edward VII Peninsula and was succeeded by a period of slow cooling until the present (Figure 3). By the time when enhanced cooling terminated, the samples have cooled to near-surface temperatures of 20–50 °C, indicating low Cenozoic exhumation rates and net exhumation values of 2.3–0.6 km for the Edward VII Peninsula and 2.0–0.4 km for the Ford Ranges (for geothermal gradients of 20–45 °C/km). Similar data were obtained for Cenozoic net exhumation from the Hobbs Coast, Kohler Range, Pine Island Bay, and Thurston Island area (Lindow et al., 2016; Spiegel et al., 2016; Zundel et al., 2019). Thus, such low exhumation rates could be explained by a scenario of tectonic quiescence and a lack of significant relief and erosion (e.g., Rohrmann et al., 2012). The change from enhanced to slow cooling is interpreted to mark the time of erosion surface formation. We therefore conclude that erosion surfaces were likely to form after ~70 Ma in the Ford Ranges and after ~60 Ma on Edward VII Peninsula. Onset of erosion surface formation in western MBL after 70–60 Ma is therefore in contradiction with the proposed formation of the WAES between 85 and 75 Ma (LeMasurier & Landis, 1996). Moreover, Figure 4b shows thermal models of adjacent areas in West Antarctica from the literature, these models indicate cessation of enhanced cooling at ~55 Ma (eastern MBL), ~50 Ma (Pine Island Bay), and ~60 Ma (Thurston Island). Together with the data of this study, a crude time progression of erosion surface formation from west to east and from ~70 to 50 Ma is recognized (Figure 4b). Thus, erosion surface formation occurred well after continental breakup and is therefore

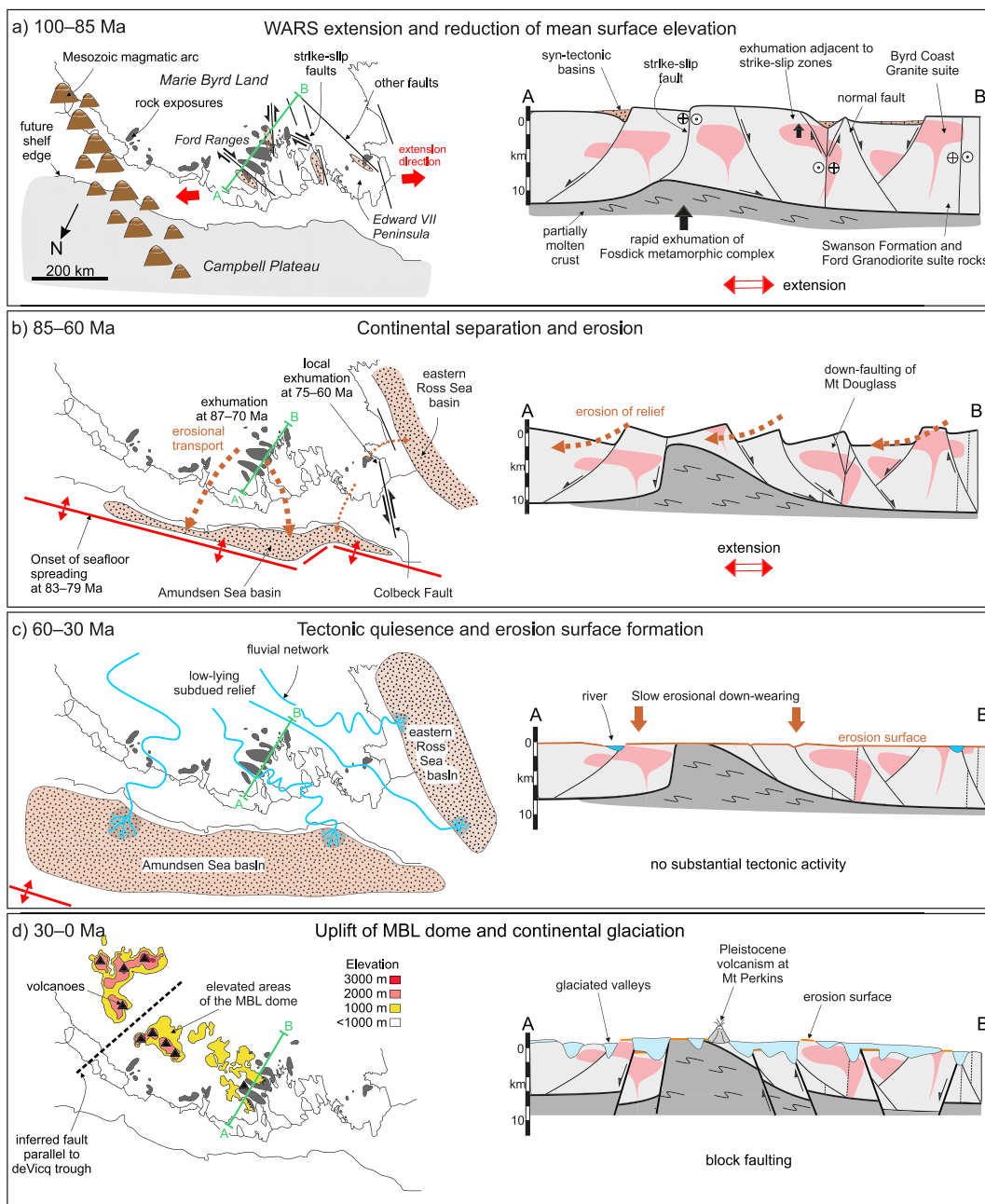


Figure 5. Panels illustrate tectonic and topographic evolution of western Marie Byrd Land since the mid-Cretaceous based on thermal history models and on literature data for four time intervals (a-d). Left-hand panels show western Marie Byrd Land and adjacent areas in map view, panels on the right show simplified geological profiles drawn along the green lines indicated in respective left panel. Note that offshore basins and continental ice-cover were omitted in left panel of time interval (d).

independent of formation of erosion surfaces in Zealandia (see Landis et al., 2008). Most strikingly, however, a time-progressive formation of erosion surfaces in West Antarctica precludes the concept that the WAES formed as a single contiguous surface at the same time. We envision formation of erosion surfaces in West Antarctica in a low-lying, tectonically inactive landscape at or slightly above sea level while a network of meandering rivers may have drained the MBL crustal block (Figure 5c). Renewed relief formation since ~30 Ma, associated with tectonic activity and uplift of the MBL dome, marks the end of erosion surface formation. Vertical block movements since ~30 Ma displaced erosion surfaces as parts of the former WAES are nowadays detected in shallow marine environments offshore MBL, where they have been subject to post-Oligocene marine erosion (Wilson & Luyendyk, 2006).

5.4. Post-Eocene Exhumation

Thermal history models show no significant change in cooling since ~60 Ma. Such a change would indicate a response to uplift of the MBL dome, to onset of glacial erosion, or to Neogene Ross Sea rifting. Thus, we conclude that neither of the processes listed above caused the exposure of reset AHe dates, which would require >1.5–0.7 km of exhumation (for geothermal gradients of 20–45 °C/km). Notably, uplift and/or erosion of the MBL dome were either too low or absent in western MBL, implying that exhumation related to dome uplift was restricted to central MBL and thus had only minor effects at the dome margins. An explanation for restricted dome uplift is that western MBL was decoupled from central MBL by a major crustal structure such as the DeVicq trough which forms a deep lineament at a high angle to the coast of MBL (Figures 1a and 5d; Holschuh et al., 2014). Decoupling from central MBL may be supported by the fact that the elevated remnants of the WAES lie at elevations <1,000 m west of the DeVicq trough and up to 2,700 m east of it (LeMasurier & Landis, 1996).

Neogene Ross Sea rifting had also no substantial effects on exhumation in western MBL and was thus prevalent in the western Ross Sea Embayment (Cande et al., 2000). Absence of considerable Neogene rift activity in western MBL may provide a reason for less dramatic ice losses compared to eastern MBL, for example, Pine Island Glacier, Thwaites Glacier, and Kohler-Smith Pope Glaciers (Pritchard et al., 2009; Rignot et al., 2008). This is because rift structures are known to act as pathways along which relatively warm ocean water can penetrate into the continental interior and melt the glaciers from below (Bingham et al., 2012; Jenkins et al., 2010; Jordan et al., 2010). Based on the thermal history models, glacial erosion in western MBL was most likely limited to valley incision in the hard granitic basement along tectonic lineaments while the intermediate high-standing nunataks experienced only minor down-wearing and thus low exhumation (Figure 5d).

Post-Eocene net exhumation in western MBL of <1.5 km (for geothermal gradients of 20–45 °C/km) cannot account for large volumes of post-Eocene sediments accumulated offshore in the Amundsen Sea basin (Figure 1a; e.g., Lindeque et al., 2016). Despite the large uncertainties of the sediments volumes in the Amundsen Sea basin, such a mismatch suggests substantial sediment supply from along shore coastal transport or from other onshore Antarctic source areas, for example, the Transantarctic Mountains, which were exhumed in Eocene-Oligocene times (Prenzel et al., 2013, 2014).

6. Conclusion

- i Thermal history models together with literature data show that western MBL underwent rapid cooling from temperatures >800 °C to <100 °C during the interval ~105–80 Ma which corresponds to oblique crustal extension of the WARS and rapid exhumation due to erosion and tectonic displacements.
- ii The overall cooling pattern of the Edward VII Peninsula and the Ford Ranges is consistent with patterns in eastern MBL and the Thurston Island block, >1,200 km to the east. The timing differs, however, as a result of cessation of oblique subduction during the Cretaceous (e.g., Sutherland & Hollis, 2001) followed by onset of seafloor spreading.
- iii Thermal history models constrain the earliest formation of the WAES to 70–60 Ma in western MBL. Our results indicate that the WAES did not form in response to a single erosional event but formed diachronously across West Antarctica, presumably propagating from west to east.
- iv Based on our thermochronological results, exhumation response to MBL dome uplift in western MBL was <1.5 km, suggesting that western MBL may have been decoupled from dome uplift in central MBL by major crustal structures. Erosion associated with the onset of Antarctic glaciation is not recorded within the sensitivity levels provided by the LT thermochronology applied in this study.

References

- Adams, C. J., Land, V., & Island, S. (1986). Geochronological studies of the Swanson Formation of Marie Byrd Land, West Antarctica, and correlation with northern Victoria Land, East Antarctica, and South Island, New Zealand. *New Zealand Journal of Geology and Geophysics*, 29(3), 345–358. <https://doi.org/10.1080/00288306.1986.10422157>
- Adams, C. J., Seward, D., & Weaver, S. D. (1995). Geochronology of Cretaceous granites and metasedimentary basement on Edward VII Peninsula, Marie Byrd Land, West Antarctica. *Antarctic Science*, 7(3), 265–276. <https://doi.org/10.1017/S095410209500037X>
- Arndt, J. E., Schenke, H. W., Jakobsson, M., Nitsche, F. O., Buys, G., Goleby, B., et al. (2013). The International Bathymetric Chart of the Southern Ocean (IBCSO) Version 1.0—A new bathymetric compilation covering circum-Antarctic waters. *Geophysical Research Letters*, 40, 3111–3117. <https://doi.org/10.1002/grl.50413>

Acknowledgments

This study has greatly benefitted from reviews of F. Korhonen and C. Siddoway who are gratefully acknowledged. C. Faccenna and J. Goodge are thanked for editorial handling. Thanks are also due to A. Toltz (University of Bremen) for sample processing. We thank the Federal Institute for Geosciences and Natural Resources (BGR) for participation in the GANOVEX VII expedition. The German Science Foundation (DFG) is acknowledged for providing financial support, Grant SP673/15-1, in the framework of the priority program SPP 1158 “Antarctic Research with comparative investigations in Arctic ice areas.” The data used are listed in the references, figures, tables, in the supporting information, and in the information system PANGAEA (<https://doi.pangaea.de/10.1594/PANGAEA.905544>).

- Barker, P. F., & Camerlenghi, A. (2002). Glacial history of the Antarctic Peninsula from Pacific margin sediments. *Proceedings of the Ocean Drilling Program, Scientific Results*, 178, 1–40, (College Station, TX: Ocean Drilling Program). Retrieved from http://www.academia.edu/download/35601354/Barker_and_Camarlenghi_2002_Glacial_Historu_of_the_Sntartic_Peninsula_From_Pacific_Margin_Sediments.PDF
- Barker, P. F., Diekmann, B., & Escutia, C. (2007). Onset of Cenozoic Antarctic glaciation. *Deep-Sea Research Part II: Topical Studies in Oceanography*, 54(21–22), 2293–2307. <https://doi.org/10.1016/j.dsr2.2007.07.027>
- Bingham, R. G., Ferraccioli, F., King, E. C., Larter, R. D., Pritchard, H. D., Smith, A. M., & Vaughan, D. G. (2012). Inland thinning of West Antarctic Ice Sheet steered along subglacial rifts. *Nature*, 487(7408), 468–471. <https://doi.org/10.1038/nature11292>
- Brown, C. R., Yakymchuk, C., Brown, M., Fanning, C. M., Korhonen, F. J., Piccoli, P. M., & Siddoway, C. S. (2016). From source to sink: Petrogenesis of cretaceous anatexitic granites from the Fosdick migmatite-granite complex, West Antarctica. *Journal of Petrology*, 57(7), 1241–1278. <https://doi.org/10.1093/petrology/egw039>
- Cande, S. C., & Stock, J. M. (2004). Constraints on Late Cretaceous and Cenozoic extension in the Ross Sea from the southwest Pacific plate circuit. In AGU Fall Meeting Abstracts.
- Cande, S. C., Stock, J. M., Müller, R. D., & Ishihara, T. (2000). Cenozoic motion between east and west Antarctica. *Nature*, 404, 145–150. <https://doi.org/10.1038/35004501>
- Candeia, P. A. (1997). A review of shallow, ore-related granites: Textures, volatiles, and ore metals. *Journal of Petrology*, 38(12), 1619–1633.
- Carlson, W. D., Donelick, R. A., & Ketcham, R. A. (1999). Variability of apatite fission-track annealing kinetics: I. Experimental results. *American Mineralogist*, 84(9), 1213–1223. <https://doi.org/10.2138/am-1999-0901>
- Carter, A., Riley, T. R., Hillenbrand, C.-D., & Rittner, M. (2017). Widespread Antarctic glaciation during the Late Eocene. *Earth and Planetary Science Letters*, 458, 49–57.
- Contreras, A. A., Siddoway, C. S., Reiners, P. W., & Gehrels, G. E. (2011). New insights on the timing and extent of Cretaceous exhumation in the West Antarctic rift system, from U-Pb and (U-Th)/He Zircon analysis. In 2011 GSA Annual Meeting in Minneapolis.
- Dalziel, I. W. D., & Elliot, D. H. (1982). West Antarctica: Problem child of Gondwanaland. *Tectonics*, 1(1), 3–19. <https://doi.org/10.1029/TC001i001p00003>
- Davy, B. (2014). Rotation and offset of the Gondwana convergent margin in the New Zealand region following Cretaceous jamming of Hikurangi Plateau large igneous province subduction. *Tectonics*, 33, 1577–1595. <https://doi.org/10.1002/2014TC003629>
- Davy, B., Hoernle, K., & Werner, R. (2008). Hikurangi Plateau: Crustal structure, rifted formation, and Gondwana subduction history. *Geochemistry, Geophysics, Geosystems*, 9, Q07004. <https://doi.org/10.1029/2007GC001855>
- Donelick, R. A., O'Sullivan, P. B., & Ketcham, R. A. (2005). Apatite fission-track analysis. *Reviews in Mineralogy and Geochemistry*, 58(1), 49–94. <https://doi.org/10.2138/rmg.2005.58.3>
- Dunkl, I. (2002). TRACKKEY: a Windows program for calculation and graphical presentation of fission track data. *Computers & Geosciences*, 28(1), 3–12.
- Eagles, G., Gohl, K., & Larter, R. D. (2004). High-resolution animated tectonic reconstruction of the South Pacific and West Antarctic Margin. *Geochemistry, Geophysics, Geosystems*, 5, Q07004. <https://doi.org/10.1029/2003GC000657>
- Farley, K. A. (2000). Helium diffusion from apatite: General behavior as illustrated by Durango fluorapatite. *Journal of Geophysical Research*, 105(B2), 2903–2914. <https://doi.org/10.1029/1999JB900348>
- Farley, K. A., Wolf, R. A., & Silver, L. T. (1996). The effects of long alpha-stopping distances on (U-Th)/He ages. *Geochimica et Cosmochimica Acta*, 60(21), 4223–4229. [https://doi.org/10.1016/S0016-7037\(96\)00193-7](https://doi.org/10.1016/S0016-7037(96)00193-7)
- Ferraccioli, F., Bozzo, E., & Damaske, D. (2002). Aeromagnetic signatures over Western Marie Byrd Land provide insight into magmatic arc basement, mafic magmatism and structure of the Eastern Ross Sea Rift flank. *Tectonophysics*, 347(1–3), 139–165. [https://doi.org/10.1016/S0040-1951\(01\)00242-6](https://doi.org/10.1016/S0040-1951(01)00242-6)
- Flowers, R. M., Ketcham, R. A., Shuster, D. L., & Farley, K. A. (2009). Apatite (U-Th)/He thermochronometry using a radiation damage accumulation and annealing model. *Geochimica et Cosmochimica Acta*, 73(8), 2347–2365. <https://doi.org/10.1016/j.gca.2009.01.015>
- Flowers, R. M., Shuster, D. L., Wernicke, B. P., & Farley, K. A. (2007). Radiation damage control on apatite (U-Th)/He dates from the Grand Canyon region, Colorado Plateau. *Geology*, 35(5), 447–450. <https://doi.org/10.1130/G23471A.1>
- Flowers, R. M., & Kelley, S. A. (2011). Interpreting data dispersion and “inverted” dates in apatite (U-Th)/He and fission-track datasets: An example from the US midcontinent. *Geochimica et Cosmochimica Acta*, 75(18), 5169–5186.
- Fretwell, P., Pritchard, H. D., Vaughan, D. G., Bamber, J. L., Barrand, N. E., Bell, R., et al. (2013). Bedmap2: Improved ice bed, surface and thickness datasets for Antarctica. *Cryosphere*, 7(1), 375–393. <https://doi.org/10.5194/tc-7-375-2013>
- Galbraith, R. F. (1981). On statistical models for fission track counts. *Journal of the International Association for Mathematical Geology*, 13(6), 471–478.
- Galeotti, S., DeConto, R., Naish, T., Stocchi, P., Florindo, F., Pagani, M., et al. (2016). Antarctic Ice Sheet variability across the Eocene-Oligocene boundary climate transition. *Science*, 352(6281), 76–80. <https://doi.org/10.1126/science.aab0669>
- Gohl, K., Denk, A., Eagles, G., & Wobbe, F. (2013). Deciphering tectonic phases of the Amundsen Sea Embayment shelf, West Antarctica, from a magnetic anomaly grid. *Tectonophysics*, 585, 113–123. <https://doi.org/10.1016/j.tecto.2012.06.036>
- Green, P. F. (1981). A new look at statistics in fission-track dating. *Nuclear Tracks*, 5(1–2), 77–86.
- Holschuh, N., Pollard, D., Alley, R. B., & Anandakrishnan, S. (2014). Evaluating Marie Byrd Land stability using an improved basal topography. *Earth and Planetary Science Letters*, 408, 362–369. <https://doi.org/10.1016/j.epsl.2014.10.034>
- Ivany, L. C., Van Simaeys, S., Domack, E. W., & Samson, S. D. (2006). Evidence for an earliest Oligocene ice sheet on the Antarctic Peninsula. *Geology*, 34(5), 377–380. <https://doi.org/10.1130/G22383.1>
- Jenkins, A., Dutrieux, P., Jacobs, S. S., McPhail, S. D., Perrett, J. R., Webb, A. T., & White, D. (2010). Observations beneath Pine Island Glacier in West Antarctica and implications for its retreat. *Nature Geoscience*, 3(7), 468–472. <https://doi.org/10.1038/ngeo890>
- Jordan, T. A., Ferraccioli, F., Vaughan, D. G., Holt, J. W., Corr, H., Blankenship, D. D., & Diehl, T. M. (2010). Aerogravity evidence for major crustal thinning under the Pine Island Glacier region (West Antarctica). *Bulletin of the Geological Society of America*, 122(5–6), 714–726. <https://doi.org/10.1130/B26417.1>
- Ketcham, R., Carter, A., Donelick, R., Baraband, J., & Hurford, A. (2007a). Improved measurement of fission-track annealing in apatite using c-axis projection. *American Mineralogist*, 92(5–6), 789–798.
- Ketcham, R. A. (2005). Forward and inverse modeling of low-temperature thermochronometry data. *Reviews in Mineralogy and Geochemistry*, 58(1), 275–314. <https://doi.org/10.2138/rmg.2005.58.11>

- Ketcham, R. A., Carter, A., Donelick, R. A., Barbarand, J., & Hurford, A. J. (2007b). Improved modeling of fission-track annealing in apatite. *American Mineralogist*, 92(5–6), 799–810. <https://doi.org/10.2138/am.2007.2281>
- Ketcham, R. A., Gautheron, C., & Tassan-Got, L. (2011). Accounting for long alpha-particle stopping distances in (U-Th-Sm)/He geochronology: Refinement of the baseline case. *Geochimica et Cosmochimica Acta*, 75(24), 7779–7791. <https://doi.org/10.1016/j.gca.2011.10.011>
- Korhonen, F. J., Brown, M., Grove, M., Siddoway, C. S., Baxter, E. F., & Inglis, J. D. (2012). Separating metamorphic events in the Fosdick migmatite-granite complex, West Antarctica. *Journal of Metamorphic Geology*, 30(2), 165–192. <https://doi.org/10.1111/j.1525-1314.2011.00961.x>
- Korhonen, F. J., Saito, S., Brown, M., Siddoway, C. S., & Day, J. M. D. (2010). Multiple generations of granite in the Fosdick Mountains, Marie Byrd Land, West Antarctica: Implications for polyphase intracrustal differentiation in a continental margin setting. *Journal of Petrology*, 51(3), 627–670. <https://doi.org/10.1093/petrology/egp093>
- Kula, J., Tulloch, A., Speli, T. L., & Wells, M. L. (2007). Two-stage rifting of Zealandia-Australia-Antarctica: Evidence from 40Ar/39Ar thermochronometry of the Sisters shear zone Stewart Island, New Zealand. *Geology*, 35(5), 411–414. <https://doi.org/10.1130/G23432A.1>
- Landis, C. A., Campbell, H. J., Begg, J. G., Mildenhall, D. C., Paterson, A. M., & Trewick, S. A. (2008). The Waipounamu Erosion Surface: Questioning the antiquity of the New Zealand land surface and terrestrial fauna and flora. *Geological Magazine*, 145(02), 173–197. <https://doi.org/10.1017/S0016756807004268>
- Larter, R. D., Cunningham, A. P., Barker, P. F., Gohl, K., & Nitsche, F. O. (2002). Tectonic evolution of the Pacific margin of Antarctica 1. Late Cretaceous tectonic reconstructions. *Journal of Geophysical Research*, 107(B12), 2345. <https://doi.org/10.1029/2000JB000052>
- Lawver, L. A., & Gahagan, L. M. (1994). Constraints on timing of extension in the Ross Sea region. *Terra Antarctica*, 1, 545–552.
- LeMasurier, W. E. (2008). Neogene extension and basin deepening in the West Antarctic rift inferred from comparisons with the East African rift and other analogs. *Geology*, 36(3), 247–250. <https://doi.org/10.1130/G24363A.1>
- LeMasurier, W. E., & Landis, C. A. (1996). Mantle-plume activity recorded by low-relief erosion surfaces in West Antarctica and New Zealand. *Geological Society of America Bulletin*, 108(11), 1450–1466. [https://doi.org/10.1130/0016-7606\(1996\)108<1450:MPARBL>2.3.CO;2](https://doi.org/10.1130/0016-7606(1996)108<1450:MPARBL>2.3.CO;2)
- LeMasurier, W. E., & Rocchi, S. (2005). Terrestrial record of post-eocene climate history in marie byrd land, west antarctica. *Geografiska Annaler: Series A, Physical Geography*, 87(1), 51–66.
- Lindeque, A., Gohl, K., Henrys, S., Wobbe, F., & Davy, B. (2016). Seismic stratigraphy along the Amundsen Sea to Ross Sea continental rise: A cross-regional record of pre-glacial to glacial processes of the West Antarctic margin. *Palaeogeography, Palaeoclimatology, Palaeoecology*, 443, 183–202. <https://doi.org/10.1016/j.palaeo.2015.11.017>
- Lindow, J., Castex, M., Wittmann, H., Johnson, J. S., Lisker, F., Gohl, K., & Spiegel, C. (2014). Glacial retreat in the Amundsen Sea sector, West Antarctica: First cosmogenic evidence from central Pine Island Bay and the Kohler Range. *Quaternary Science Reviews*, 98, 166–173. <https://doi.org/10.1016/j.quascirev.2014.05.010>
- Lindow, J., Kamp, P. J. J., Mukasa, S. B., Kleber, M., Lisker, F., Gohl, K., et al. (2016). Exhumation history along the eastern Amundsen Sea coast, West Antarctica, revealed by low-temperature thermochronology. *Tectonics*, 35, 2239–2257. <https://doi.org/10.1002/2016TC004236>
- Lisker, F., & Olesch, M. (1998). Cooling and denudation history of western Marie Byrd Land, Antarctica, based on apatite fission-tracks. In *Advances in Fission-Track Geochronology* (pp. 225–240). https://doi.org/10.1007/978-94-015-9133-1_14
- Lisker, F., Ventura, B., & Glasmacher, U. A. (2009). Apatite thermochronology in modern geology. *Geological Society, London, Special Publications*, 324(1), 1–23. <https://doi.org/10.1144/SP324.1>
- Luyendyk, B. (1995). Hypothesis for Cretaceous rifting of east Gondwana caused by subducted slab capture. *Geology*, 23(4), 373–376. Retrieved from <http://geology.gsapubs.org/content/23/4/373.short>
- Luyendyk, B. P., Sorlien, C. C., Wilson, D. S., Bartek, L. R., & Siddoway, C. S. (2001). Structural and tectonic evolution of the Ross Sea rift in the Cape Colbeck region, Eastern Ross Sea, Antarctica. *Tectonics*, 20(6), 933–958. Retrieved from <https://doi.org/10.1029/2000TC001260/full>
- Luyendyk, B. P., Wilson, D. S., & Siddoway, C. S. (2003). Eastern margin of the Ross Sea Rift in western Marie Byrd Land, Antarctica: Crustal structure and tectonic development. *Geochemistry, Geophysics, Geosystems*, 4(10), 1090. <https://doi.org/10.1029/2002GC000462>
- McFadden, R. R., Siddoway, C. S., Teyssier, C., & Fanning, C. M. (2010). Cretaceous oblique extensional deformation and magma accumulation in the Fosdick Mountains migmatite-cored gneiss dome, West Antarctica. *Tectonics*, 29, TC4022. <https://doi.org/10.1029/2009TC002492>
- McFadden, R. R., Teyssier, C., Siddoway, C. S., Cosca, M. A., & Fanning, C. M. (2015). Mid-Cretaceous oblique rifting of West Antarctica: Emplacement and rapid cooling of the Fosdick Mountains migmatite-cored gneiss dome. *Lithos*, 232, 306–318. <https://doi.org/10.1016/j.lithos.2015.07.005>
- Mukasa, S. B., & Dalziel, I. W. D. (2000). Marie Byrd Land, West Antarctica: Evolution of Gondwana's Pacific margin constrained by zircon U-Pb geochronology and feldspar common-Pb isotopic compositions. *Bulletin of the Geological Society of America*, 112(4), 611–627.
- Müller, R. D., Gohl, K., Cande, S. C., Goncharov, A., & Golynsky, A. V. (2007). Eocene to Miocene geometry of the West Antarctic rift system. *Australian Journal of Earth Sciences*, 54(8), 1033–1045. <https://doi.org/10.1080/08120090701615691>
- Pankhurst, R., Weaver, S., & Bradshaw, J. (1998). Geochronology and geochemistry of pre-Jurassic superterrane in Marie Byrd Land, Antarctica. *Journal of Geophysical Research*, 103(97), 2529–2547. <https://doi.org/10.1029/97jb02605>
- Poole, I., Cantrill, D., & Uttescher, T. (2005). A multi-proxy approach to determine Antarctic terrestrial palaeoclimate during the Late Cretaceous and Early Tertiary. *Palaeogeography, Palaeoclimatology, Palaeoecology*, 222(1–2), 95–121. <https://doi.org/10.1016/j.palaeo.2005.03.011>
- Prenzel, J., Lisker, F., Balestrieri, M. L., Läufer, A., & Spiegel, C. (2013). The Eisenhower Range, Transantarctic Mountains: Evaluation of qualitative interpretation concepts of thermochronological data. *Chemical Geology*, 352, 176–187. <https://doi.org/10.1016/j.chemgeo.2013.06.005>
- Prenzel, J., Lisker, F., Elsner, M., Schöner, R., Balestrieri, M. L., Läufer, A. L., et al. (2014). Burial and exhumation of the Eisenhower range, transantarctic mountains, based on thermochronological, sedimentary rock maturity and petrographic constraints. *Tectonophysics*, 630(C), 113–130. <https://doi.org/10.1016/j.tecto.2014.05.020>
- Pritchard, H. D., Arthern, R. J., Vaughan, D. G., & Edwards, L. A. (2009). Extensive dynamic thinning on the margins of the Greenland and Antarctic ice sheets. *Nature*, 461(7266), 971–975. <https://doi.org/10.1038/nature08471>

- Richard, S. M., Smith, C. H., Kimbrough, D. L., Fitzgerald, P. G., Luyendyk, B. P., & McWilliams, M. O. (1994). Cooling history of the northern Ford Ranges, Marie Byrd Land, West Antarctica. *Tectonics*, 13(4), 837–857. <https://doi.org/10.1029/93TC03322>
- Rignot, E., Bamber, J. L., van den Broeke, M. R., Davis, C., Li, Y., van de Berg, W. J., & van Meijgaard, E. (2008). Recent Antarctic ice mass loss from radar interferometry and regional climate modelling. *Nature Geoscience*, 1(2), 106–110. <https://doi.org/10.1038/ngeo102>
- Rohrmann, A., Kapp, P., Carrapa, B., Reiners, P. W., Guynn, J., Ding, L., & Heizler, M. (2012). Thermochronologic evidence for plateau formation in central Tibet by 45 Ma. *Geology*, 40(2), 187–190.
- Siddoway, C. S. (2008). Tectonics of the West Antarctic rift system: New light on the history and dynamics of distributed intracontinental extension. Antarctica: A Keystone in a Changing World - Online Proceedings of the 10th ISAES, 91–114. <https://doi.org/10.3133/of2007-1047.kp09>
- Siddoway, C. S., Baldwin, S. L., Fitzgerald, P. G., Fanning, C. M., & Luyendyk, B. P. (2004a). Ross sea mylonites and the timing of intra-continental extension within the West Antarctic rift system. *Geology*, 32(1), 57–60. <https://doi.org/10.1130/G20005.1>
- Siddoway, C. S., & Fanning, C. M. (2009). Paleozoic tectonism on the East Gondwana margin: Evidence from SHRIMP U-Pb zircon geochronology of a migmatite-granite complex in West Antarctica. *Tectonophysics*, 477(3–4), 262–277. <https://doi.org/10.1016/j.tecto.2009.04.021>
- Siddoway, C. S., Richard, S. M., Fanning, C. M., & Luyendyk, B. P. (2004b). Origin and emplacement of a middle Cretaceous gneiss dome, Fosdick Mountains, West Antarctica. *GSA*, 267–294. <https://doi.org/10.1130/0-8137-2380-9.267>
- Siddoway, C. S., Sass, L. C., & Esser, R. P. (2005). Kinematic history of western Marie Byrd Land, West Antarctica: Direct evidence from Cretaceous mafic dykes. *Terrane Processes at the Margins of Gondwana*, 246, 417–438. <https://doi.org/10.1144/gsl.sp.2005.246.01.17>
- Smith, C. (1996). Migmatites of the Alexandra Mountains, West Antarctica: Pressure-temperature conditions of formation and regional context. *Geologisches Jahrbuch*, B, 169–178.
- Spell, T. L., McDougall, I., & Tulloch, A. J. (2000). Thermochronologic constraints on the breakup of the Pacific Gondwana margin: The Paparoa metamorphic core complex, South Island, New Zealand. *Tectonics*, 19(3), 433–451.
- Spiegel, C., Kohn, B., Belton, D., Berner, Z., & Gleadow, A. (2009). Apatite (U-Th-Sm)/He thermochronology of rapidly cooled samples: The effect of He implantation. *Earth and Planetary Science Letters*, 285(1–2), 105–114. <https://doi.org/10.1016/j.epsl.2009.05.045>
- Spiegel, C., Lindow, J., Kamp, P. J. J., Meisel, O., Mukasa, S., Lisker, F., et al. (2016). Tectonomorphic evolution of Marie Byrd Land: Implications for Cenozoic rifting activity and onset of West Antarctic glaciation. *Global and Planetary Change*, 145, 98–115. <https://doi.org/10.1016/j.gloplacha.2016.08.013>
- Stone, J. O., Balco, G. A., Sugden, D. E., Caffee, M. W., Sass, L. C., Cowdery, S. G., & Siddoway, C. (2003). Holocene deglaciation of Marie Byrd land, west Antarctica. *Science*, 299(5603), 99–102. <https://doi.org/10.1126/science.1077998>
- Storey, B. C., Leat, P. T., Weaver, S. D., Pankhurst, R. J., Bradshaw, J. D., & Kelley, S. (1999). Mantle plumes and Antarctica-New Zealand rifting: Evidence from mid-Cretaceous mafic dykes. *Journal of the Geological Society*, 156(4), 659–671. <https://doi.org/10.1144/gsjgs.156.4.0659>
- Summerfield, M. A., & Brown, R. W. (1998). Geomorphic factors in the interpretation of fission-track data. In *Advances in Fission-Track Geochronology* (pp. 269–284). https://doi.org/10.1007/978-94-015-9133-1_17
- Sutherland, R., & Hollis, C. (2001). Cretaceous demise of the Moa plate and strike-slip motion at the Gondwana margin. *Geology*, 29(3), 279–282.
- Wagner, G., Michalski, I., & Zaun, P. (1989). Apatite fission track dating of the Central European basement. Postvariscan thermo-tectonic evolution. The German Continental Deep Drilling. Retrieved from http://link.springer.com/chapter/10.1007/978-3-642-74588-1_19
- Weaver, S. D., Adams, C. J., Pankhurst, R. J., & Gibson, I. L. (1992). Granites of Edward VII Peninsula, Marie Byrd Land: Anorogenic magmatism related to Antarctic–New Zealand rifting. In *Transactions of the Royal Society of Edinburgh: Earth Sciences* (Vol. 83, pp. 281–290). <https://doi.org/10.1130/spe272-p281>
- Weaver, S. D., Storey, B. C., Pankhurst, R. J., Mukasa, S. B., DiVenere, V. J., & Bradshaw, J. D. (1994). Antarctica-New Zealand rifting and Marie Byrd Land lithospheric magmatism linked to ridge subduction and mantle plume activity. *Geology*, 22, 811–814. Retrieved from <http://geology.gsapubs.org/content/22/9/811.short>
- Wilson, D. S., & Luyendyk, B. P. (2006). Bedrock platforms within the Ross Embayment, West Antarctica: Hypotheses for ice sheet history, wave erosion, Cenozoic extension, and thermal subsidence. *Geochemistry, Geophysics, Geosystems*, 7, Q12011. <https://doi.org/10.1029/2006GC001294>
- Wilson, D. S., Pollard, D., Deconto, R. M., Jamieson, S. S. R., & Luyendyk, B. P. (2013). Initiation of the West Antarctic Ice Sheet and estimates of total Antarctic ice volume in the earliest Oligocene. *Geophysical Research Letters*, 40, 4305–4309. <https://doi.org/10.1002/grl.50797>
- Wilson, D. S., & Luyendyk, B. P. (2009). West antarctic paleotopography estimated at the Eocene-Oligocene climate transition. *Geophysical Research Letters*, 36, L16302. <https://doi.org/10.1029/2009GL039297>
- Winberry, J. P., & Anandakrishnan, S. (2004). Crustal structure of the West Antarctic rift system and Marie Byrd Land hotspot. *Geology*, 32(11), 977–980. <https://doi.org/10.1130/G20768.1>
- Wolf, R. A., Farley, K. A., & Kass, D. M. (1998). Modeling of the temperature sensitivity of the apatite (U-Th)/He thermochronometer. *Chemical Geology*, 148, 105–114. [https://doi.org/10.1016/S0009-2541\(98\)00024-2](https://doi.org/10.1016/S0009-2541(98)00024-2)
- Yakymchuk, C., Brown, C. R., Brown, M., Siddoway, C. S., Fanning, C. M., & Korhonen, F. J. (2015). Paleozoic evolution of western Marie Byrd Land, Antarctica. *Bulletin of the Geological Society of America*, 127(9–10), 1464–1484. <https://doi.org/10.1130/B31136.1>
- Yakymchuk, C., Siddoway, C. S., Fanning, C. M., McFadden, R. R., Korhonen, F. J., & Brown, M. (2013). Anatexitic reworking and differentiation of continental crust along the active margin of Gondwana: A zircon Hf-O perspective from West Antarctica. *Geological Society Special Publication*, 383, 169–210. <https://doi.org/10.1144/sp383.7>
- Zachos, J., Pagani, M., Sloan, L., Thomas, E., & Billups, K. (2001). Trends, rhythms, and aberrations in global climate 65 Ma to present. *Science*, 292(5517), 686–693. <https://doi.org/10.1126/science.1059412>
- Zundel, M., Spiegel, C., Mehling, A., Lisker, F., Hillenbrand, C. D., Monien, P., & Klügel, A. (2019). Thurston Island (West Antarctica) between Gondwana subduction and continental separation: A multistage evolution revealed by apatite thermochronology. *Tectonics*, 38, 878–897. <https://doi.org/10.1029/2018TC005150>

References From the Supporting Information

- Adams, C. J. (1987). Geochronology of granite terranes in the Ford Ranges, Marie Byrd Land, West Antarctica. *New Zealand Journal of Geology and Geophysics*, 30, 54–72. <https://doi.org/10.1080/00288306.1987.10422193>
- Dumitru, T. A. (1993). A new computer-automated microscope stage system for fission-track analysis. *International Journal of Radiation Applications and Instrumentation. Part, 21*(4), 575–580. [https://doi.org/10.1016/1359-0189\(93\)90198-I](https://doi.org/10.1016/1359-0189(93)90198-I)
- Farley, K. A. (2002). (U-Th)/He dating: Techniques, calibrations, and applications. *Reviews in Mineralogy and Geochemistry*, 47(1), 819–844. <https://doi.org/10.2138/rmg.2002.47.18>
- Hurford, A. J., & Green, P. F. (1983). The zeta age calibration of fission-track dating. *Chemical Geology*, 41, 285–317.
- Laslett, G. M., Kendall, W. S., & Gleadow, A. J. W. (1982). Bias in the measurement of fission track length distributions. *Nuclear Tracks*, 6, 79–85. Retrieved from <http://www.sciencedirect.com/science/article/pii/0735245X8290031X>
- Slater, T., Shepherd, A., McMillan, M., Muir, A., Gilbert, L., Hogg, A. E., et al. (2018). A new digital elevation model of Antarctica derived from CryoSat-2 altimetry. *The Cryosphere*, 12(4), 1551–1562. <https://doi.org/10.5194/tc-12-1551-2018>